Monatsh Chem 139, 373–387 (2008)
DOI 10.1007/s00706-007-0828-6
Printed in The Netherlands

Monatshefte für Chemie
Chemical Monthly

Review

Adsorption and reaction of organic molecules on solid surfaces – *ab-initio* density functional investigations

Jürgen Hafner

Faculty of Physics, Universität Wien and Center for Computational Materials Science, Wien, Austria

Received 28 August 2007; Accepted 15 October 2007; Published online 14 March 2008

Abstract The state-of-the-art of density-functional studies of the adsorption and reaction of organic molecules on solid surfaces is illustrated at three examples chosen to cover different aspects of the field. The first concerns the adsorption and subsequent hydrogenation of benzene on nickel surfaces. Here the essential points are the description of the adsorption geometry and the determination of the barriers and heats of reaction for the hydrogenation to cyclohexene. It is shown that although in the gas-phase, the energy differences between the different cyclic hydrocarbon species are correctly described only at the level of a meta-generalized-gradient-approximation (meta-GGA) to the exchange-correlation functional (providing an improved description of electron localization in double bonds), for the adsorbed species a conventional GGA leads to accurate geometries and energetics. The second example serves to study the interplay between surface reconstruction and the molecular geometry of the adsorbate. It is demonstrated that the buckling of the Si–Si dimers in the Si(100) surface (and the associated charging of the surface Si atoms) has a decisive influence on the energetically most favorable adsorption configuration of acrylonitrile, based on the resonant form of the molecule with cumulative C=C and C=N double bonds. As the formation of the energetically most favorable configuration involves a complex rearrangement of the adsorbate, it is argued that kinetic effects are also essential for interpreting the experimental information. The third case study describes the *Beckmann* rearrangement of cyclohexanone oxime to ε-caprolactam catalyzed by an acid zeolite. It is shown that, in combination with harmonic transition-state theory, the DFT calculations allow to uniquely identify *Brønsted* acid sites as the catalytically active center. Finally we discuss briefly the current status of the implementation of the hierarchy of DFT functionals and their application to the interaction between molecules and solids (with particular reference to the performance of hybrid functionals) and attempts to include entropic effects in the *ab-initio* modeling of catalyzed molecular reactions.

Keywords Density functional theory; Chemisorption; Catalytic reactions; Zeolites; Transition-state theory.

Introduction

The adsorption of organic molecules on solid surfaces and their chemical reactions catalyzed by the contact with these surfaces are of growing interest because of the fundamental importance of an improved understanding of the interaction and bonding mechanism between organic films and metallic or insulating substrates. A deeper understanding of these interactions is also of technological importance

Correspondence: Jürgen Hafner, Faculty of Physics, Universität Wien and Center for Computational Materials Science, Sensengasse 8, A-1090 Wien, Austria. E-mail: juergen.hafner@univie.ac.at

in various fields, ranging from catalysis to the emerging molecular electronics. During the last decade, the development of efficient and accurate density-functional methods has substantially increased the potential of theoretical studies to contribute to a solution of this complex problem. In this paper I shall illustrate the state of the art in this field at three illustrative examples. (i) The adsorption and hydrogenation of benzene on the low-index surfaces of nickel. Evidently the interest in this problem is motivated by the importance of nickel and similar metals as catalysts for hydrogenation and ring-cracking reactions. The benzene/metal complex has been studied extensively in the past using a variety of experimental techniques [1, 2], while progress in theory was rather slow due to the computational effort associated with the large cells required to simulate adsorbed monolayers of large molecules such as benzene even at saturation coverage. (ii) The adsorption of acrylonitrile at the Si(100) surface. The attachment of organic molecules to semiconductor surfaces is considered as an important step towards the development of molecular electronics [3]. This problem is of considerable complexity because of the large number of possible adsorption configurations of a multifunctional molecule on the reconstructed Si surface [4]. The goal of theoretical studies is to establish and to explain the energetic hierarchy of configurations. (iii) The *Beckmann* rearrangement of cyclohexanone oxime to ε-caprolactam, catalyzed by *Brønsted* acid sites located either in the cavities or at the outer surface of a zeolite. This reaction is an important step in the production of nylon. The industrial process uses sulfuric acid as catalysts, but for environmental reasons extensive efforts are being undertaken to replace this by a gas-phase process catalyzed by a zeolite [5, 6]. The aim of the theoretical studies is to determine a realistic scenario for the reaction and to elucidate the nature of the active site.

The paper is organized as follows: In Sect. 2 we review very briefly the methodology used for solving the *Kohn-Sham* equation of density-functional theory, for the structural optimization of the adsorbate/substrate complex, for transition-state searches and for the calculation of reaction rates. Section 3 describes the adsorption of benzene on close-packed Ni surfaces and its stepwise hydrogenation. In Sect. 4 we present the investigation of acrylonitrile adsorption on Si(100), Sect. 5 is devoted to the modellization of the gas-phase *Beckmann* rearrangement of cyclohexanone oxime to ε-caprolactam, catalyzed by different active sites in the pores or on the outer surface of a zeolite. We summarize in Sect. 6, together with an outlook on recent developments.

Computational method

All calculations discussed here have been performed using the Vienna *ab-initio* simulation package VASP [7, 8]. VASP performs an iterative solution of the *Kohn-Sham* equations of density functional theory (DFT) using residuum minimization techniques and optimized charge-density mixing routines. The program uses a plane-wave basis set, electron-ion interactions are described within the projector-augmented wave (PAW) scheme [9, 10]. The advantage of using a plane-wave basis set (typical cut-off energies range between 350 and 450 eV) is that it allows an efficient control of basis-set convergence and an easy access to the calculation of the *Hellmann-Feynman* forces acting on the atoms and of the stresses on the unit cell. The PAW method reconciles the efficiency of a pseudopotential approach with the accuracy of the most advanced all-electron techniques.

An essential point of all DFT calculations is the choice of an exchange-correlation functional. The local density approximation (LDA) is notorious for its tendency to overbind, producing too large binding energies and too short interatomic distances. The various flavors of the generalized gradient approximation (GGA) such as the *Perdew-Wang* (*PW*) [11] or the *Perdew-Burke-Ernzerhof* (*PBE*) [12] functionals quite efficiently cure the overbinding tendency. Although the adsorption energy of molecules on solid surfaces can be overestimated by as much as 0.3 eV, the activation energies for molecular reactions are generally determined with very good accuracy. Attempts to improve upon the GGA functionals have been made in two different directions: Meta-GGA functionals [13] introduce a dependence on the local kinetic energy density of the electrons (or the *Laplacian* of the electron density), in addition to a dependency on the local electron density and its gradient; while hybrid functionals [14–18] mix DFT exchange with non-local *Hartree-Fock* (*HF*) exchange. Meta-GGA functionals lead in some cases to an improved description of the energetics – but the improvement is not really systematic. Hybrid functionals are now the standard for DFT calculations in molecular quantum chemistry based on local

basis sets, but their application to complex solids became possible only with the recent implementation in the plane-wave based VASP code [19, 20]. The results available so far demonstrate that their performance on solids is ambiguous – which is in some cases not so surprising because some hybrid functionals fail to meet the correct limiting free-electron behavior. While for semiconductors and insulators the prediction of energy-gaps and related properties is greatly improved over conventional calculations with GGA functionals [20], their performance on metallic systems is rather disappointing, the admixture of *HF* exchange leading to too large band widths and for magnetic systems to a dramatic overestimation of the magnetic moments and of the exchange splitting [20, 21]. Most of the results discussed here are based on GGA functionals, including spin-polarization effects where required. Post-GGA corrections are briefly mentioned where appropriate.

The adsorbate/substrate complex is modelled by a periodically repeated supercell, consisting of several layers of the substrate and a surface cell large enough to model the system at saturation coverage (for benzene on Ni(111), *e.g.*, this leads to a surface cell with seven Ni atoms per layer). The simulations of the *Beckmann* rearrangement have been performed for mordenite – a zeolite with channels and cavities wide enough to accommodate the large reactant molecules. The orthorhombic unit cell of mordenite contains 144 atoms, to avoid lateral interactions the unit cell has been doubled in the direction of the shortest lattice vector. The *Brillouin*-zone integrations have been performed on *Monkhorst-Pack* [22] grids chosen corresponding to the size of the unit cell, using a modest smearing of the eigenvalues to improve convergence [23].

Vibrational eigenstates of solids, isolated molecules or of the adsorbate/substrate complex can either be derived by *Fourier*-transforming the velocity autocorrelation function (VACF) calculated in an *ab-initio* molecular-dynamic run or by diagonalization of the dynamical matrix calculated using a finite-difference approach [24].

Transition-states for chemical reactions of molecules chemisorbed at the outer surface of a solid have been determined using the nudged-elastic band method [25]. This method is based on a mapping of the minimum-potential-energy path connecting two local minima (representing reactant and product states) by a simultaneous relaxation of a series of intermediate states in the hyperspace perpendicular to the reaction coordinate. For the rather loosely bound molecules in the cavity of a zeolite the structures of transition states are identified using a ''drag'' method [26] modified for the use of internal coordinates [27]. Reaction rates have been calculated within harmonic transition-state theory [28], using vibrational eigenfrequencies derived *via* a finite-difference method [24].

So far most transition-state calculations are based on the determination of the potential-energy barrier using static relaxation methods. Transition-state searches based on the calculation of free-energy barriers can be performed *via* constrained *Monte-Carlo* [29] or molecular-dynamics methods in combination with thermodynamic integration [30], but the application of these methods in combination with *ab-initio* DFT calculations [31, 32] is still in its infancy due to the huge computational effort.

Adsorption and hydrogenation of benzene on Ni(111)

The adsorption and successive hydrogenation of benzene is not only a model system for hydrotreating reactions of aromatic compounds, it is also a fundamental process in the refining industry as for environmental reasons strict limitations have been imposed to the benzene content of gasoline. Catalysts based on supported group VIII metals such as Pt, Pd or Ni are under consideration as efficient catalysts for the hydrogenation of aromatics. However, although the adsorption and heterogeneous hydrogenation of benzene over Ni has been well studied for some time [1, 2, 33, 34], important aspects remain unclear. At lower coverage, on Ni(111) adsorption takes place over a bridge site, while at saturation on the basis of the interpretation of angular-resolved photoemission spectra a change to hollow adsorption has been claimed [2]. High-resolution low-energy energy-loss spectroscopy (HREELS) in combination with low energy electron diffraction (LEED) [33] yields a lower R-factor for bridge-adsorption – but this result has been dismissed because the data also imply an unrealistically large distortion of the molecular geometry. The heterogeneous hydrogenation of benzene has been studied extensively [34, 35], but important aspects of the reaction kinetics remain unclear, the reported activation energies range from 0.26 to 0.97 eV [34].

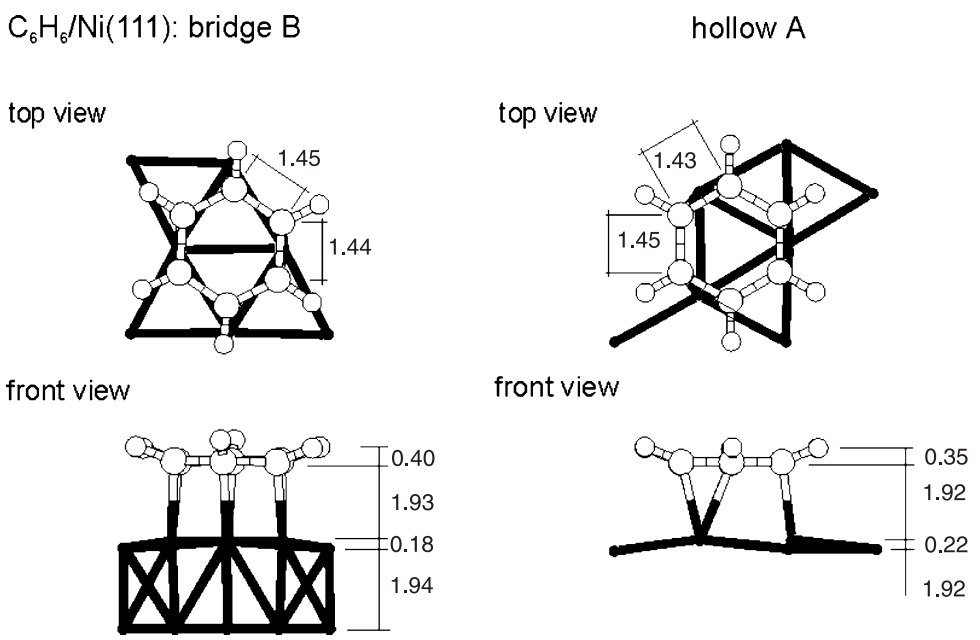

Fig. 1 Optimized adsorption geometry for benzene adsorbed on Ni(111) in a bridge position (adsorption energy 1.00 eV) and in a hollow position (adsorption energy 0.94 eV). All distances are given in Å. After *Mittendorfer* and *Hafner*, Ref. [36]

Adsorption of benzene on Ni surfaces

Mittendorfer and *Hafner* [36, 37] have presented detailed DFT studies of the adsorption and hydrogenation of benzene on the low-index surfaces of Ni. For the (111) surface the studies have been performed for a $\sqrt{7}\times\sqrt{7}$ surface cell corresponding to the low-temperature saturation coverage and a slab consisting of four monolayers of Ni. For this cell, *Brillouin* zone integrations have been performed using a $4\times4\times1$ M*onkhorst-Pack* grid [22] and a *Methfessel-Paxton* smearing [23] of the eigenvalues of 0.1 eV. Atomic positions in the two top layers of the substrate have been allowed to relax. A similar set-up was used for the other low-index surfaces. The calculations have been performed with and without spin-polarization.

On the (111) surface the two energetically most favorable adsorption sites are the bridge position with the C–H bonds perpendicular to the Ni rows ($E_{ad} = 1.00\,\text{eV/molecule}$) and the hollow position with C–H bonds parallel to the Ni-rows ($E_{ad} = 0.94\,\text{eV/molecule}$). In both cases the molecule lies parallel to the surface, at a distance of 1.92 Å, and with only a modest distortion of the molecular geometry (see Fig. 1), in very good agreement with the results of the photoelectron diffraction [38] but contradicting the HRLEED analysis predicting a distorted molecular geometry [33]. In the bridge configuration two Ni atoms form strong two-center bonds with individual carbon atoms, while the remaining two Ni atoms bind to two C–C pairs. In the hollow configuration three equivalent bonds between Ni atoms and C–C pairs of the aromatic ring are formed. The electronic properties reflect the different bonding geometries: Bonds between Ni atoms and C–C pairs are promoted by the t_{2g}–p_z overlap (maximized by a canting of the C-p orbitals resulting also in a tilting of the C–H bonds away from the surface), while the two-center Ni–C bonds are based on the overlap of $d_z{}^2$ and p_z orbitals. The differences in the re-hybridization of the molecular eigenstates also lead to a splitting of the $3e_{2g}$ state for the bridge, but not in the hollow configuration which is also observed in the photoemission spectra [1]. The analysis of the vibrational spectrum of the adsorbed molecule shows that the stronger tilting of the C–H bonds in the bridge configuration (see Fig. 1) leads to a stronger shift of the C–H stretching modes, in agreement with the results of electron-energy loss spectroscopy (EELS) [39]. On the other hand, the predicted shift of the C–C frequencies (reflecting a weakening of the bond in the aromatic ring) is predicted to be stronger for hollow-adsorbed benzene, again in agreement with the EELS data.

The magnetism of the substrate has a very modest effect on the adsorption properties, although the adsorption of benzene leads to a strong reduction of the magnetic moments of the Ni atoms forming bonds with the C atoms in the aromatic ring (the magnetic moment of these atoms is reduced to $0.32\,\mu_B$ com-

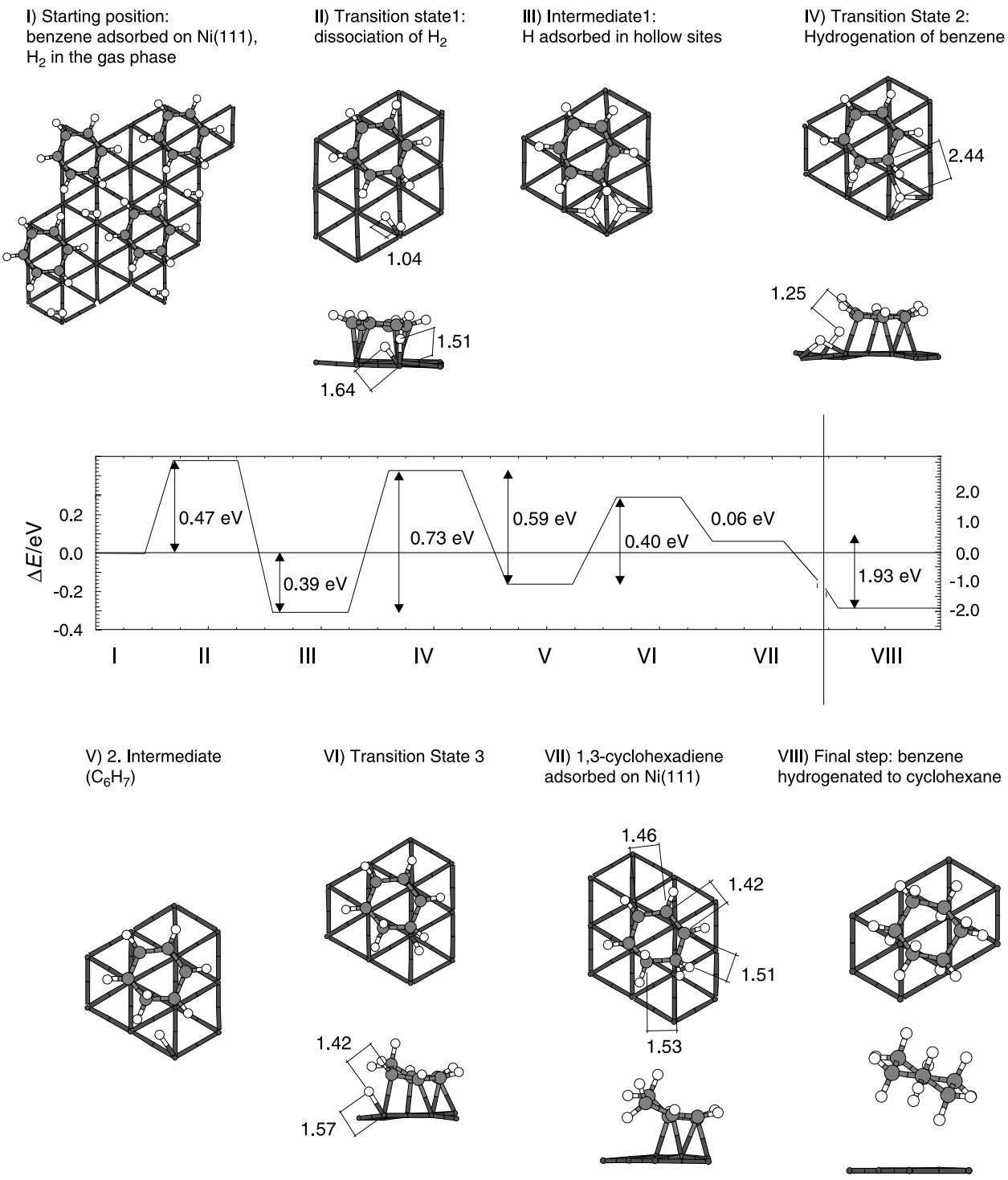

Fig. 2 Potential-energy profile for the hydrogenation of benzene adsorbed on a Ni(111) surface according to a *Langmuir-Hinshelwood* mechanism. Starting from pre-adsorbed benzene (I), a hydrogen molecule is adsorbed dissociatively on the surface (II and III), followed by a stepwise hydrogenation of the benzene molecule (IV–VII). Hydrogenated to cyclohexane, the molecule is only weakly physisorbed on the surface. After *Mittendorfer* and *Hafner*, Ref. [37]

pared to $0.68\,\mu_B$ for a Ni atom on a clean (111) surface). The energy difference for adsorption in bridge and hollow sites is reduced to 0.04 eV (compared to 0.06 eV without spin-polarization), Ni–C bond lengths increase by 0.01 Å for bridge and by 0.02 Å for hollow adsorption.

On the Ni(100) surface benzene is strongly adsorbed ($E_{ad} = 2.13$ eV) in a hollow position, because this configuration allows to form four C–Ni bonds without an appreciable distortion of the molecule. The adsorption strength on the Ni(110) surface is intermediate between the strong bonding on the (100) and the relatively weak bonding on the (111) surface, because four C–Ni bonds of approximately equal strength can be formed only if the aromatic ring is tilted against the surface and undergoes a modest distortion [36]. The predicted adsorption geometry is in good agreement with STM [40] and photoelectron diffraction [41] investigations.

Hydrogenation of benzene to cyclohexadiene catalyzed by Ni

The initial stages of the hydrogenation of benzene to cyclohexane, catalyzed by Ni, have been investigated by *Mittendorfer* and *Hafner* [37]. The starting state is benzene bridge-adsorbed on Ni(111) and molecular hydrogen in the gas phase. The coverage assumed in this simulation corresponds to the experimentally determined saturation coverage. The potential-energy profile for the first reaction steps – coadsorption and dissociation of H_2, hydrogenation of C_6H_6 to C_6H_7, second hydrogenation to cyclohexadiene – according to a *Langmuir-Hinshelwood* reaction between the co-adsorbed species is shown in Fig. 2. The reaction barriers have been calculated using the nudged-elastic-band method [25]. The most important results may be summarized as follows: (i) At this high surface coverage, dissociation of hydrogen is an activated process with a barrier of 0.47 eV, while on a clean Ni(111) surface hydrogen dissociation is non-activated [42]. At lower coverage, the barrier for this step will be determined by the diffusion of atomic hydrogen on the surface (activation energy 0.15 eV). (ii) The rate-controlling step is the first hydrogenation of benzene (true activation energy 0.73 eV – in good agreement with the experimental estimates), with a rather late transition-state at a small C–H distance of 1.25 Å between a C atom of the ring and the added hydrogen atom. (iii) The barriers for the successive hydrogenation steps are significantly reduced, the transition-state for the second step is found already at a C–H distance of 1.47 Å. (iv) Adsorbed 1,3-cyclohexadiene is lower in energy by 0.22 eV than 1,4-cyclohexadiene (which is more stable in the gas phase). (v) For a *Eley-Rideal* reaction between adsorbed benzene and a hydrogen molecule from the gas-phase, the activation energy is 2.8 eV. This activation energy can be considered as a lower limit for a gas-phase reaction – hence the Ni catalyst reduces the barrier for benzene hydrogenation by at least 2 eV.

The difficult point in this analysis is that although DFT calculations based on conventional GGA functionals (*PW* or *PBE*) predict the molecular geometries with high accuracy, they lead for molecules in the gas-phase to significantly too large energy differences of the unsaturated cyclic hydrocarbons (benzene, cyclohexadiene, cyclohexene) relative to cyclohexane, the error increases with the number of C=C double bonds from 0.25 eV for cyclohexene to 0.66 eV for benzene [43]. Calculations with a meta-GGA functional [13] lead to significantly improved energy differences (the error is reduced to 0.01/0.04/0.17 eV for cyclohexene, cyclohexadiene, and benzene). These results indicate that the correction terms to the GGA functional containing the kinetic energy density greatly improve the prediction of the energetic difference between single and double bonds. For the activation energies of the reactions catalyzed by the contact with the metal surface, however, the changes resulting from the choice of the exchange-correlation functional are much less dramatic (the largest change of 0.06 eV is found for the activation energy of the second hydrogenation step). This reflects the fact that due to the interaction with the substrate, the difference between a single and a double bond and between aromatic and non-aromatic behaviour is significantly reduced.

In summary we find that GGA functionals allow for a quite accurate determination of the geometry and energetics of the adsorption of aromatic molecules on metallic surfaces and that due to the interaction with the substrate the predicted energy difference between the various species of adsorbed cyclic hydrocarbons is significantly more accurate than in the gas phase.

Adsorption of acrylonitrile on the Si(100) surface

The adsorption of acrylonitrile (CH_2=CH–C≡N) on a Si(100) surface is a model system for the investigation of the growth of organic arrays on the structured surface of a semiconductor, with evident implications for the fundamental aspects of molecular electronics. Due to the necessity to saturate the dangling bonds at the surface, a bare Si(100) surface undergoes a (2×1) reconstruction leading to the formation of rows of asymmetric, slightly buckled dimers linked by Si=Si double bonds (see Fig. 3). The reconstruction is well described by DFT [44] and quantum *Monte-Carlo* [45] calculations, while quantum-chemical calculations at the post-*Hartree-Fock* level fail to reproduce the buckling [46]. The reason for these conflicting results is that the buckling is essentially a *Jahn-Teller* distortion induced by the coupling of occupied and empty surface states across the gap, whose width is overestimated by *Hartree-Fock* and post-*Hartree-Fock* calculations. The asymmetry of the dimers leads to a transfer of a fraction of one electron from the down to the up atom in the dimer, which is an important factor in determining the adsorption geometry. The acrylonitrile molecule with its seven atoms and its ground-state configuration with a conjugate π system and a resonant form with cumulative C=C and C=N double bonds (involving a shift of the electron density from the carbon towards the nitrogen end, see Scheme 1) is a good choice to extract the essential features of bonding to Si surfaces. For this reason, a number of experimental [47–49] and theoretical [50–52] studies have been devoted to this system. Possible adsorption configurations involve cycloaddition to a single Si–Si dimer, either *via* the terminal atoms or *via* the C=C and C=N π-bonds [53]. However, recent studies [47, 48, 50, 54] predict bonding *via* Si atoms belonging to different dimers to be more favorable.

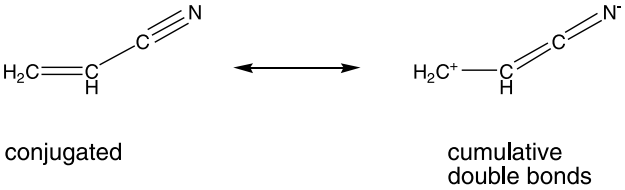

Scheme 1

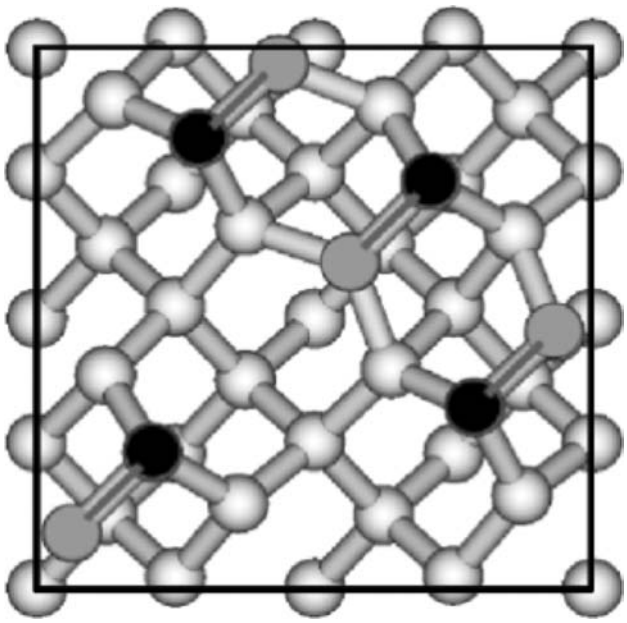

Fig. 3 Optimized surface cell of Si(100) showing two parallel rows of buckled Si–Si dimers. Dark circles represent electron-enriched Si atoms in an up position

Extensive *ab-initio* DFT studies involving a large number of different configurations have recently been performed by *Cobian et al.* [53, 54]. The calculations use the *PW*-GGA functional proposed by *Perdew et al.* [11] and (4×2) surface cells large enough to permit the investigation of configurations where the adsorbed molecule span over the trench separating two parallel rows of Si dimers ("cross-trench" configurations). The slab representing the surface contains seven layers of Si, six of them have been allowed to relax. The use of a rather thick slab is mandatory, because as a consequence of the angular stiffness of the Si–Si bonds, the surface reconstruction extends to deeper layers.

The adsorption configurations considered in these studies are (ordered according to the number of adsorbate/substrate bonds): (i) One-bond configurations: Bonding *via* the N- or the CH_2-end of the molecule to one Si atom. (ii) Two-bond configurations. These involve cycloadditions [bonding to a single Si–Si dimer at the surface *via* the C=C or the C=N double bond (configurations $[2+2]_{CC}$ and $[2+2]_{CN}$) or *via* the terminal atoms of the cumulative form of the molecule (configuration $[4+2]$)], cross-dimer and cross-trench configurations binding *via* the terminal atoms to Si atoms in two different dimers belonging to the same (cross-dimer) or neighboring (cross-trench) dimer rows. (iii) Tripod configurations allowing the formation of two C–Si and one N–Si bonds. (iv) Tetrapods where the atoms of the molecule bind to four Si atoms in two different dimers. The energetic hierarchy of all configurations

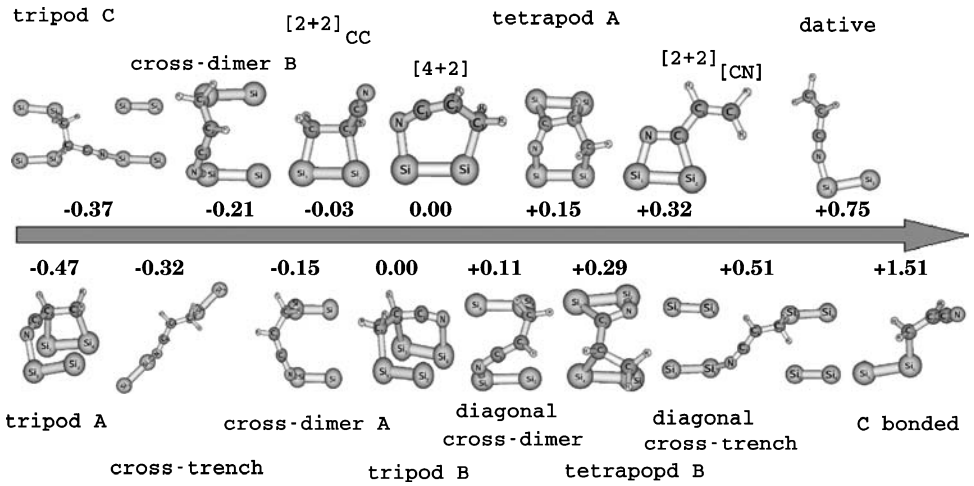

Fig. 4 Energetic hierarchy of the adsorption configurations of acrylonitrile on Si(100). All energy differences are quoted relative to the [4 + 2] cycloaddition (adsorption energy 1.81 eV). *Cf.* text. After *Cobian et al.*, Ref. [54]

is summarized in Fig. 4. The energetic ordering of the different adsorption configurations results from two competing effects: (i) A deformation of both the molecule and of the adsorbate is required to allow the formation of adsorbate/substrate bonds. (ii) The bond formation energy which increases with the number of adsorbate/substrate bonds.

In general, the stability of a configuration increases with the number of bonds built with the surface: Tripods A and C are much more stable than the related diagonal cross-dimer and diagonal cross-trench configurations (see Fig. 4). Tetrapods however are energetically unfavorable because they require a too large deformation of the adsorbate and also of the lattice. The most stable configuration is tripod A, for which Fig. 5 shows the difference electron density visualizing the formation of adsorbate/substrate bonds. The reference configurations are the distorted substrate without the adsorbate and the isolated distorted resonant form of acrylonitrile with cumulative C=C and C=N double bonds, for which separate selfconsistent calculations have been performed. Hence the charge-flow represented in Fig. 5 reflects the chemical bonding between adsorbate and substrate. The charge redistribution demonstrates (i) the formation of three σ bonds between the N, C_2, and C_3 atoms of the molecule and the Si atoms at the surface, (ii) a weakening of the C_2–C_3 bond, (iii) a reinforcement of the bonding between the C_1 and C_2 atoms, (iv) stronger back-bonds between the Si atoms binding to the molecule and the underlying lattice, and (v) an increased polarity of the C–N bond. To adapt the molecule to this configuration requires an energy of 2.15 eV, the distortion of the lattice about 0.64 eV, but this energy loss is overcompensated by the energy gain of −5.07 eV by forming three strong adsorbate-substrate bonds so that the adsorption is exothermic by −2.28 eV. Tetrapods lead to a larger energy gain by bond-formation, but their formation requires strong angular deformations of both the adsorbate and the lattice, costing too much energy.

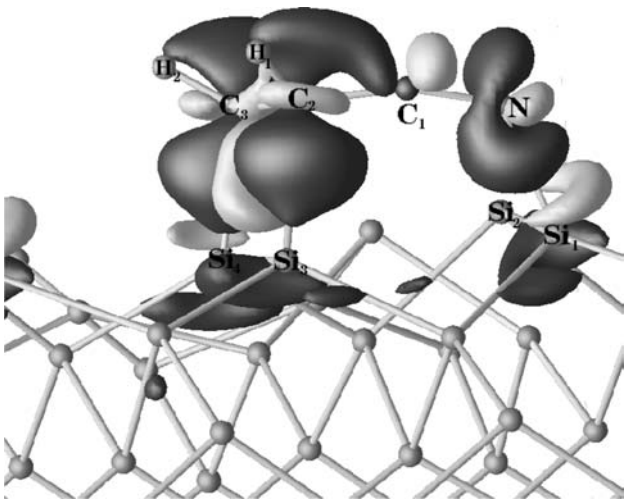

Fig. 5 Difference electron density (equidensity surfaces) for the adsorption of acrylonitrile on Si(100) in the Tripod A configuration forming two Si–C bonds and one Si–N bonds. Dark areas represent electron accumulation (enhanced bonding), light areas electron depletion (bond weakening). After *Cobian et al.*, Ref. [54]

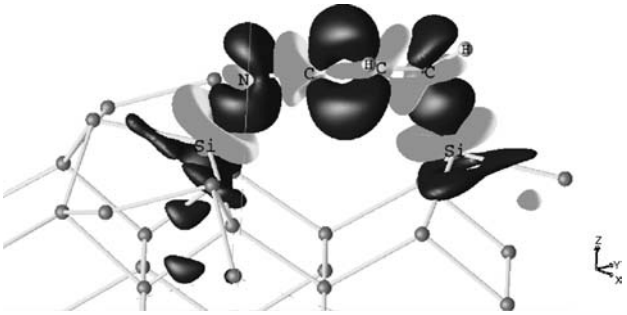

Fig. 6 Difference electron density (equidensity surfaces) for the adsorption of acrylonitrile on Si(100) in the "cross-trench" configuration, binding *via* the terminal atoms to Si atoms belonging to dimers in two different rows. Dark areas represent electron accumulation, light areas electron depletion. After *Cobian et al.*, Ref. [54]

However, so far no experimental evidence for the existence of this configuration has been reported. The formation of a tripod is probably kinetically hindered because a precursor to this geometry is a diagonal cross-dimer configuration (see Fig. 4) in which both ends of the molecule bind to Si atoms carrying the same charge, leading to a dipole-mismatch with the cumulative form of acrylonitrile. Excluding the tripod configurations, the most stable configuration is the cross-trench configuration in which the adsorbate bridges the through between two parallel dimer rows. The difference electron density for this adsorption configuration is shown in Fig. 6. The charge-redistribution illustrates: (i) The formation of two σ-bonds between the terminal N and C atoms of the adsorbate and Si atoms in two neighboring dimer rows. Note that the Si atoms carry different charges, combining favorably with the charges on the C and N atoms of the cumulative form of acrylonitrile. (ii) The reduction of the triple C≡N bond to a double bond. (iii) The formation of a new $C_1{=}C_2$ double bond, with a clear signature of π bonding. (iv) The reduction of the double $C_2{=}C_3$ double bond to a single bond. For the other simple bridging structures the energetic ordering (cross trench → cross dimer → diagonal cross dimer → diagonal cross trench) corresponds to the sequence expected on the basis of geometrical considerations and of the dipole/dipole interactions between adsorbate and surface dimers. The cross-trench configuration agrees with the interpretation of the observations by scanning tunnelling microscopy [48] and by photoemission and infrared spectroscopies [49] at low coverages. With increasing coverage the situation becomes very complex and the available experiments have been tentatively interpreted also in terms of other configurations, including some of the bridging configurations [47–49]. However, the DFT calculations demonstrate that these configurations ($[2+2]_{CC}$ and $[4+2]$) are penalized by at least 0.3 eV/molecule relative to the more favorable cross-trench configuration.

In summary, this study has shown that: (i) The buckling of the Si dimers plays a key role in determining the adsorption configurations of acrylonitrile on Si(100), both by disfavoring certain configurations energetically and by kinetically hindering the formation of energetically favorable structures because the transition states involve unfavorable dipole configurations. (ii) Among the configurations compatible with the surface dipoles carried by the Si dimers and with the same number of adsorbate substrate bonds those imposing the minimal distortions on the adsorbed molecule are favored.

Vapor-phase *Beckmann* rearrangement catalyzed by acid sites in a zeolite

The *Beckmann* rearrangement (*B*R) is a reaction in which oximes are transformed to the corresponding amides. An industrially important application is the conversion of cyclohexanone oxime to ε-caprolactam (Scheme 2). Usually this reaction is carried out in sulfuric acid – this is problematic from the environmental point of view and also unsatisfactory because of a low selectivity. It has been proposed to replace the conventional process by a vapor-phase reaction catalyzed by an acidic zeolite [5, 6]. Various zeolites, including mordenite and ferrierite have been tested, but there is still ongoing dispute on the nature of the catalytically active sites. *Hölderich* and co-workers [5, 55] suggested that the active sites are silanol nests (*i.e.*, structural defects formed upon removing a tetrahedral site from the zeolite framework and saturation of the dangling bonds of the four surrounding oxygen atoms by hydrogen), while isolated

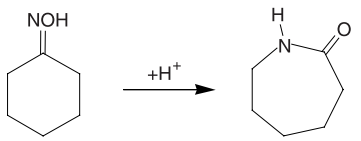

Scheme 2

terminal silanol groups at the outer surface are reported to be inactive. In contrast, *Corma et al.* [56] claimed that the *B*R is catalyzed by strong acid sites. *Nguyen et al.* [57] proposed a scenario for the *B*R in which the role of the catalyst is reduced to protonate the oxime. The reaction proceeds by the following steps: protonation of oxime → N-protonated species → 1,2-H shift → O-protonated species → migration → elimination → fragmentation products → hydrolysis → lactam. So far, theoretical studies of the *B*R have been limited either to gas-phase models assisted by strong acids such as H_2SO_4 or HCl [57, 58] or reactions catalyzed by oxide catalysts represented by cluster models [59]. Using quantum-chemical calculations at the *MP2* level *Nguyen et al.* found that for small oxime molecules the rate-determining step is the 1,2-H shift with an activation energy larger than 210 kJ/mol. DFT calculations (using a hybrid functional) for the gas-phase *B*R of cyclohexanone oxime have been performed by *Fois et al.* [58] and *Yamaguchi et al.* [60]. In agreement with *Nguyen et al.* the 1,2-H shift was found to be the rate-determining step with an activation energy of 237 kJ/mol [58] and 214 kJ/mol [60]. Much lower barriers are reported for the insertion of the N atom into the ring (about 10 kJ/mol) and for the final hydrolysis step (about 70 to 80 kJ/mol).

Extensive DFT investigations of the *B*R of cyclohexanone oxime to ε-caprolactam, in the gas-phase and catalyzed by various active sites in a zeolite, have been performed by *Bucko et al.* [61]. These investigations are based on the gradient corrected *PW* exchange-correlation functional [11]. The zeolite chosen is mordenite, an industrially important zeolite with a medium-sized unit cell (in the purely siliceous form the orthorhombic cell with lattice constants $a = b = 13.66$ Å and $c = 7.61$ Å (DFT calculations by *Demuth et al.* [62]) contains 144 atoms). To avoid interactions between molecules adsorbed in the periodically repeated unit cells, for the calculations a cell doubled in the c-direction has been adopted. Transition-state searches have been performed using the modified drag method [26, 27]. The active sites considered in this study are a *Brønsted* acid site located on the wall of the main channel of the framework (created by a Si/Al substitution on the framework and protonation of a neighboring O atom), a silanol nest, and a terminal silanol group at the outer (001) surface. The surface is modeled by a periodically repeated slab [63].

Gas-phase reaction

To create a reference, a simulation of the gas-phase reaction has been performed. Transition-state searches are performed using the drag-method [26] and a full relaxation in terms of internal coordinates [27]. Starting from the N-protonated oxime, the activation energies (corrected for zero-point energies) are 178 kJ/mol (1,2-H shift), 10 kJ/mol (insertion of N into the ring), and 54 kJ/mol (hydrolysis), in reasonable agreement with the results of *Yamaguchi et al.* [60] based on hybrid functionals.

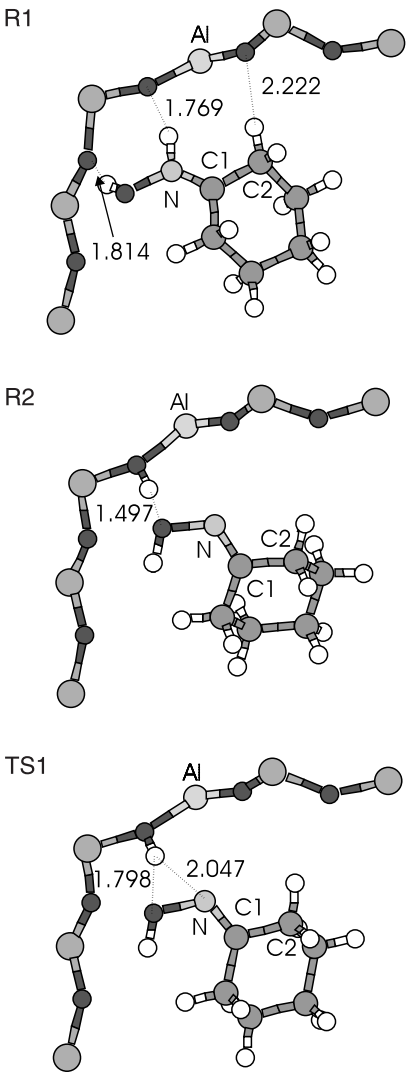

Fig. 7 N-Protonated (R1) and hydrogen-bonded (R2) adsorption complexes of cyclohexanone oxime at a *Brønsted* acid site in the main channel of mordenite, and the transition-state (TS1) for the transformation between these two configurations. Only a small part of the mordenite framework is shown. All distances are given in Å. After *Bucko et al.*, Ref. [61]

Reaction catalyzed by a Brønsted acid site

The reaction intermediates, transition-states and the chemisorbed product state for a reaction catalyzed by a *Brønsted* site are shown in Figs. 7–9. The reaction starts with the N-protonated cyclohexanone oxime, which is the most stable adsorption configuration. The 1,2-H shift is achieved by proton transfer from the N-protonated oxime to a framework oxygen atom next to the substituted Al atom on the framework, producing a hydrogen-bonded oxime (see Fig. 7). The activation energy for this process is 88 kJ/mol, *i.e.*, reduced by 90 kJ/mol compared to the gas-phase reaction. A similar lowering of the activation energy has been reported by *Nguyen et al.* [64] for the 1,2-H shift of protonated formaldehyde oxime catalyzed by sulfuric acid. In the transition-state for N-insertion the proton is transferred from the *Brønsted* acid site to the hydroxyl group of the reactant. This results in the dissociation of a water molecule which is hydrogen-bonded to a framework oxygen, see Fig. 8. The calculated activation energy for this step is 64 kJ/mol, *i.e.*, higher by 54 kJ/mol than for the gas-phase reaction. The reason for this increase is that the interaction with the zeolite framework stabilizes the reaction intermediates more than the transition state. The dissociation of a water molecule results in the formation of a carbiminium ion with the nitrogen atom incorporated in a C_6N ring. The final reaction step is the hydrolysis of the carbiminium ion. The water molecule approaches the ion, forming a hydroxyl group binding through the O atom to the C_1 atom next to the N atom in the ring. In the transition-state the second H atom from the water molecule is located between the O and N atoms, the final product is a N-protonated ε-caprolactam (see Fig. 9). The activation energy for this step is 40 kJ/mol (14 kJ/mol lower than for the gas-phase reaction), the desorption energy of ε-caprolactam is 86 kJ/mol. A complete potential-energy profile of the reaction is

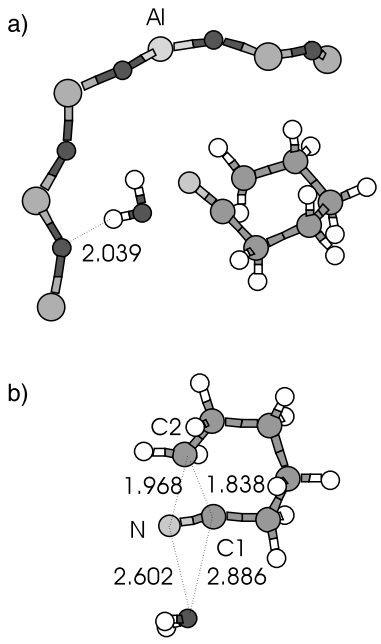

Fig. 8 (**a**) Transition state TS2 for the insertion of the nitrogen atom into the ring of the oxime molecule. (**b**) Details of the transition-state geometry. All distances are given in Å. After *Bucko et al.*, Ref. [61]

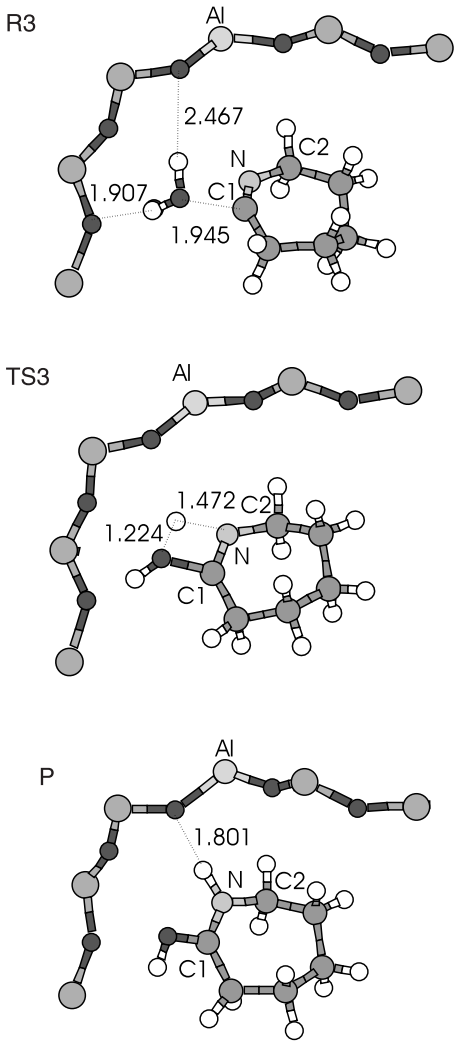

Fig. 9 Hydrolysis of the carbiminium ion created by nitrogen insertion into the C-ring: R3 – carbiminium ion and water molecule, TS3 transition state, P reaction product: N-protonated ε-caprolactam. All distances are given in Å. After *Bucko et al.*, Ref. [61]

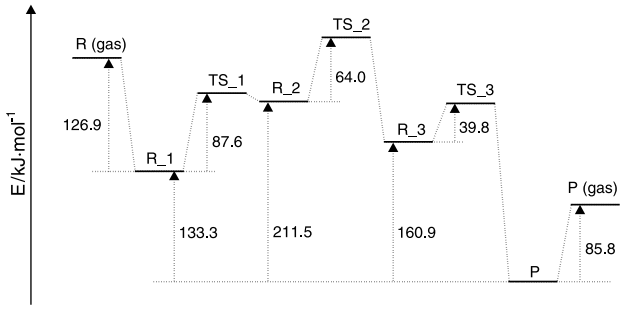

Fig. 10 Potential-energy profile for the *Beckmann* rearrangement of cyclohexanone oxime to ε-caprolactam catalyzed by a *Brønsted* acid site in mordenite. After *Bucko et al.*, Ref. [61]

shown in Fig. 10. Apart from the strong reduction of the activation energy for the first reaction step, the profile is rather similar to that for a gas-phase reaction, but in stark contrast to the results of the semi-empirical MNDO calculations of *Shinohara et al.* [65] (in which the zeolite was represented only by a small cluster) predicting activation energies of 20 kJ/mol and 327 kJ/mol for 1,2-H shift and N-insertion. The difference arises both from a low level of theory and from the neglect of the interaction with the zeolite framework which leads to a significant modification of the reaction profile.

Reaction catalyzed by silanol groups

The potential-energy profiles for reactions catalyzed by a silanol nest or a terminal silanol group are found to be very different. For the *B*R at a silanol nest the activation energies for the three steps are 42, 149, and 72 kJ/mol. The very large barrier for N-insertion results from an insufficient stabilization of the transition state by hydrogen bonds. The reaction at a pair of hydrogen-bonded terminal silanol groups at the outer surface of mordenite follows a slightly different scenario. Cyclohexanone oxime is hydrogen-bonded at the outer surface, hence the first reaction step is the N-insertion with a high activation energy of 223 kJ/mole, again resulting from an insufficient stabilization of the transition-state. This activation energy is much higher than the adsorption energy of 77 kJ/mol. The activation energy of 79 kJ/mol calculated for the final reaction step (hydrolysis) is therefore of academic interest only.

Effective reaction rates

To complete the analysis, the reaction rates for all steps (and the corresponding back-transformations) catalyzed by a *Brønsted* acid site or a silanol group have been calculated using harmonic transition-state theory [28], see Table 1. For the reaction at a *Brønsted* site the slowest reaction step is the 1,2-H shift – which is also hindered by a very fast backward reaction (which is even faster than the following reaction step, the N-insertion). For this step and for the final hydrolysis, the backward reactions are much slower than the corresponding forward steps, they can therefore be neglected. *Bucko et al.* [61] have demonstrated that the *B*R catalyzed by a *Brønsted* site is effectively an elementary first order reaction R1 → P, with an effective activation energy given by the energy difference between the highest saddle point (TS2) and the reactant, i.e. $E^{\mathrm{eff}}{}_{\mathrm{act}} \sim E_{\mathrm{act}}{}^{\mathrm{R1\text{-}R2}} + E_{\mathrm{act}}{}^{\mathrm{R2\text{-}R3}} - E_{\mathrm{act}}{}^{\mathrm{R2\text{-}R1}} \sim 142\,\mathrm{kJ/mol}$, much lower than for the gas phase reaction. The effective rate-constant is $7.1 \times 10^5\,\mathrm{sec}^{-1}$. Similar considerations for the reaction catalyzed by a silanol nest lead to an effective activation energy of 184 kJ/mol and

Table 1. Calculated zero-point energy corrected activation energies E_{act} and rate constants k (calculated at $T = 623$ K) for the *Beckmann* rearrangement of cyclohexanone oxime to ε-caprolacatam catalyzed by a *Brønsted* acid site (*B*A) and by a silanol nest

		*B*A $E_{\mathrm{act}}/\mathrm{kJ \cdot mol^{-1}}$	*B*A $k \cdot \mathrm{s}^{-1}$		Silanol nest $E_{\mathrm{act}}/\mathrm{kJ \cdot mol^{-1}}$	Silanol nest k/s^{-1}
R1 → R2	N-protonated → H-bonded	88	2.71×10^6	N-protonated → H-bonded	42	7.74×10^8
R2 → R1		9	1.37×10^{12}		7	2.53×10^{12}
R2 → R3	N-insertion	64	4.89×10^{11}	N-insertion	149	1.07×10^4
R3 → R2		115	2.22×10^6		245	1.24×10^{-4}
R3 → P	Hydrolysis of carbiminium ion	40	3.22×10^9	Lactim-lactam transformation	72	1.96×10^8
P → R3		201	1.27×10^{-2}		159	1.07×10^1

an effective rate constant of $3.3\,\mathrm{sec}^{-1}$. The reaction catalyzed by a *Brønsted* site is therefore five orders of magnitude faster than that at a silanol nest. Hence the computational modelling shows that only a *Brønsted* acid site can catalyze a *B*R in a zeolite.

Discussion and outlook

In the foregoing sections we have discussed three examples where *ab-initio* modelling has made a significant contribution to our understanding of the adsorption and reaction of molecules in contact with external and inner surfaces of solids. The first demonstrates that DFT yields an accurate description of the adsorption geometry of cylic hydrocarbons on metallic surfaces and that, even if the accuracy of the predicted energy differences between various gas-phase species based on conventional GGA functionals is limited (and can be cured only by using meta-GGA functionals accounting for the different degree of localization of electrons in single and double bonds), heats of reaction and reaction barriers for the adsorbed species calculated in a conventional GGA are more accurate. The second example shows that details of the surface reconstruction such as the buckling of the Si dimers on a Si(100) surface may be of decisive importance for assessing the stable adsorption geometry of a moderately complex organic molecule (acrylonitrile), due to the electrostatic interactions between the Si–Si dipoles and the charges on the terminal atoms of the resonant form of the molecule. The third example illustrates the state-of-the-art of periodic DFT calculation of reaction rates at the example of a complex multi-step reaction in acid catalysis. The investigation of the *Beckmann* rearrangement of cyclohexanone oxime test the ability of DFT calculations to accurately describe the chemisorption (protonation) of the reactant, the opening of the ring of the oxime molecule, and the final hydrolysis of carbiminium molecule created by the nitrogen insertion. It is demonstrated that the rate-limiting step is different for different possible active sites (*Brønsted* sites, silanol nests, terminal silanol groups), the analysis of the reaction-rates shows that only *Brønsted* sites efficiently catalyze the reaction.

However, these examples also illustrate some of the limitations of and challenges to state-of-the-art DFT calculations. The first and perhaps most widely discussed limitation is the tendency of DFT to overestimate the strength of the adsorbate/substrate interaction. This does not only lead to too large values of the adsorption energy, but in some critical cases even to the prediction of a wrong adsorption site – a well known example is that DFT calculations predict CO adsorption in the threefold hollows of the (111) surfaces of Pt, Rh, and Cu, while on-top adsorption is observed experimentally. The current consensus is that the main reason for the failure of DFT is the incorrect position of the highest occupied molecular orbital (HOMO) and of the lowest unoccupied molecular orbital (LUMO) relative to the *Fermi* energy of the metal [66]. If the HOMO–LUMO gap is corrected empirically by shifting the HOMO to higher energies by adding a *Coulomb* repulsion to the DFT Hamiltonian, the correct energetic order of the adsorption sites is indeed achieved [67, 68]. As hybrid functionals tend to correct the HOMO–LUMO gap, there was some hope that their use would solve the ''CO adsorption puzzle''. However, very recent calculations by *Stroppa et al.* [69] based on the *PBE*0 [15, 16] and *HSE*03 [17, 18] functionals (enabled by the implementation of hybrid functionals in VASP [19, 20]) demonstrated that this is not always the case. For Cu, the up-shift of the CO–LUMO is accompanied by a down-shift of the filled d-band – both effects tend to reduce the LUMO-d interaction, reducing the adsorption energy and predicting the correct on-top adsorption. For transition metals the d-band is constrained to remain at the *Fermi* level, and the non-local exchange included in a hybrid functional broadens the d-band. The increased bandwidth partially restores the strong LUMO-d interaction and hence the hybrid functionals fail to predict the correct adsorption site on Pt(111). The failure of hybrid functionals to correctly describe metallic systems is even more dramatic for magnetic systems where magnetic moments and the exchange splitting are strongly overestimated [20, 21]. This applies not only to bulk magnets, but also to magnetic ions. Recent investigations of transitions-metal exchanged microporous silico-alumino phosphates (with structures very similar to zeolites) have demonstrated that although the prediction of the energy gap is significantly improved, the overestimation of the exchange splitting of the d-states of the metallic cations significantly affects their interaction with the valence band of the host lattice and hence their chemical reactivity [70]. The conclusion is that a fixed ratio between local and non-local exchange as used in the

current hybrid functionals may be appropriate for exchange-dominated systems such as molecules and insulators, but not for metallic solids or metal ions in solids where the non-local exchange is evidently more strongly screened.

Transition-state searches based on the exploration of the potential-energy surfaces and calculations of reaction rates within harmonic transition-state theory are evidently based on the assumption that even in the transition-state the reactants is relatively strongly bound to the catalyst such that entropic effects are minimized. The *B*R of cyclohexanone oxime in mordenite discussed here may be a borderline case, as the interaction with the zeolites is largely based on hydrogen bonds. The calculation of the free-energy profile of a reaction is certainly one of the actual challenges in DFT modeling. Various techniques for the calculation of free-energy profiles have been developed, including thermodynamic integration methods [30] and metadynamics [71]. However, the combination of these methods with *ab-initio* DFT calculations for complex systems remains a very challenging task. Very recently *Bucko et al.* [31] have used *ab-initio* molecular dynamics and thermodynamic integration techniques to determine the free-energy profiles and transition states for proton exchange reactions of various hydrocarbons in an acidic zeolite. It has been demonstrated that entropic effects have a strong influence on the selectivity between proton exchange involving methyl and methylene groups of linear hydrocarbons, but do not significantly modify the height of the reaction barrier. Hence it is legitimate to expect that the barriers and reaction rates for the *B*R are reasonably accurate. A drawback of the thermodynamic integration method, however, is that it requires the choice of a reaction coordinate, and hence a knowledge of the relevant reaction mechanisms. In contrast, metadynamics [71] introducing a bias driving the system in the direction of the product state is capable of exploring new reactions mechanisms described by a set of collective variables, but here it is more difficult to estimate the statistical error in the free-energy barrier. Future progress in DFT studies of the reaction of organic molecules catalyzed by solid surfaces will undoubtedly depend (i) on the construction of accurate functionals applicable to both metallic and insulating systems and (ii) further developments of efficient algorithms for searching free-energy reaction barriers.

Acknowledgements

It is a pleasure to thank *G. Kresse*, *F. Mittendorfer*, *T. Bucko*, *G. Boureau*, and *M. Cobian* for their important contributions to the work discussed in this article.

References

1. Steinrück HP, Huber W, Pache T, Menzel D (1989) Surf Sci 218:293
2. Steinrück HP (1996) J Phys Condens Matter 8:6465
3. Bent SF (2002) Surf Sci 500:879
4. Seino K, Schmidt WG, Furthmüller J, Bechstedt F (2002) Phys Rev B 66:235323
5. Hölderich WF, Röseler J, Heitman G, Liebens AT (1997) Catal Today 37:353
6. Dai LX, Koyama K, Miyamoto M, Tatsumi T (1999) Appl Catal A 189:237
7. Kresse G, Hafner J (1994) Phys Rev B 49:14251
8. Kresse G, Furthmüller J (1996) Comput Mat Sci 6:1
9. Blöchl PE (1994) Phys Rev B 50:17953
10. Kresse G, Joubert D (1999) Phys Rev B 59:1758
11. Perdew JP, Chevary JA, Vosko SH, Jackson KA, Pedersen MR, Singh DJ, Fiolhais C (1992) Phys Rev B 46:6671
12. Perdew JP, Burke K, Ernzerhof M (1996) Phys Rev Lett 77:3865
13. Perdew JP, Kurth S, Zupan A, Blaha P (1999) Phys Rev Lett 82:2544
14. Becke AD (1993) J Chem Phys 98:5648
15. Perdew JP, Burke K, Ernzerhof M (1996) J Chem Phys 105:9982
16. Burke K, Ernzerhof M, Perdew JP (1997) Chem Phys Lett 265:115
17. Heyd J, Scuseria GE, Ernzerhof M (2003) J Chem Phys 118:8207
18. Heyd J, Scuseria GE (2004) J Chem Phys 120:7274
19. Paier J, Hirschl R, Marsman M, Kresse G (2005) J Chem Phys 122:34102
20. Paier J, Marsman M, Hummer K, Kresse G, Gerber IC, Angyan JG (2006) J Chem Phys 124:154709; Erratum ibid. 125:249901
21. Paier J, Marsman M, Kresse G (2007) J Chem Phys 127:024103
22. Monkhorst HJ, Pack JD (1976) Phys Rev B 13:5188
23. Methfessel M, Paxton A (1989) Phys Rev B 40:3616
24. Kresse G, Furthmüller J, Hafner J (1995) Europhys Lett 32:729
25. Mills G, Jonsson G (1994) Phys Rev Lett 72:1124
26. Henkelman G, Johannesson G, Jonsson H (2000) Methods for finding saddle points and minimum energy paths. In: Schwartz SD (ed) Progress in Theoretical Chemistry and Physics, Kluwer Academic Publishers, Dordrecht, p 272
27. Bucko T, Angyan JG, Hafner J (2005) J Chem Phys 122:124508
28. Van Santen RA, Niemantsverdriet HW (1995) Chemical Kinetics and Catalysis, Plenum Press, New York, p 139
29. Dellago C, Bolhuis PG, Geisler P (2002) Adv Chem Phys 123:1

30. Fleurat-Lassard P, Ziegler T (2005) J Chem Phys 123:084101
31. Bucko T, Benco L, Hafner J, Angyan JG (2007) J Catal 250:171
32. East ALL, Bucko T, Hafner J (2007) J Phys Chem 111:5945
33. Held G, Bessent MP, Titmuss S, King DA (1996) J Chem Phys 105:11305
34. Bond GC, Keane MA, Kral H, Lercher JA (2000) Catal Rev Sci Eng (2000) 42:323
35. Stanislaus A, Cooper BH (1996) Catal Rev Sci Eng 42:323
36. Mittendorfer F, Hafner J (2001) Surf Sci 472:133
37. Mittendorfer F, Hafner J (2002) J Phys Chem B 106:13299
38. Schaff O, Fernandez V, Hoffmann P, Schindler KM, Theobald A, Fritzsche V, Bradshaw AM, Davis R, Woodruff DP (1996) Surf Sci 348:89
39. Bertolini JC, Dalmai-Imelik G, Rousseau J (1977) Surf Sci 67:478
40. Doering M, Rust HP, Briner BG, Bradshaw AM (1998) Surf Sci 410:L736
41. Kang JH, Toomes RL, Robinson J, Woodruff DP, Schaff O, Terborg R, Lindsay R, Baumgärtel P, Bradshaw AM (2000) Surf Sci 448:23
42. Kresse G (2000) Phys Rev B 62:8295
43. Cox JD, Pilcher G (1970) Thermochemistry of Organic and Organometallic Compounds, Academic Press, New York
44. Krüger P, Pollmann J (1995) Phys Rev Lett 74:1155
45. Healy SB, Filippi C, Kratzer P, Penev E, Scheffler M (2001) Phys Rev Lett 87:016105
46. Jung Y, Shao Y, Gordon MS, Doren DJ, Head-Gordon M (2003) J Chem Phys 119:10917
47. Bournel F, Gallet J, Kubsky S, Dufour G, Rochet F, Simeoni M, Sirotti F (2002) Surf Sci 513:37
48. Rangan S, Kubsky S, Gallet J (2005) Phys Rev B 71:125320
49. Schwartz MP, Barlow DE, Russel JN, Butler JE, D'Evelyn MP, Hamers RJ (2005) J Am Chem Soc 127:8348
50. Choi CH, Gordon MS (2002) J Am Chem Soc 124:6162
51. Cho JH, Kleinman L (2004) J Chem Phys 121:1557
52. de Leon-Perez RMF, Ferraz AC (2004) Braz J Phys 34:708
53. Cobian M, Ilakovac V, Carniato S, Capron N, Boureau G, Hirschl R, Hafner J (2004) J Chem Phys 120:9793
54. Cobian M, Boureau G, Hafner J, Kresse J (2005) J Chem Phys 123:174705
55. Heitmann GP, Dahlhoff G, Hölderich WF (1999) J Catal 186:12
56. Camblor MA, Corma A, Garcia H, Semmer-Herledan V, Valencia V (1998) J Catal 177:267
57. Nguyen MT, Raspoet G, Vanquickenborne LG (1997) J Am Chem Soc 119:2552
58. Fois GA, Ricchiardi G, Bordiga S, Busco C, Dalloro L, Spano G, Zecchina A (2001) Proceedings of the 13th Zeolite Conference, p 149
59. Ishida M, Suzuki T, Ichihashi H, Shiga A (2003) Catal Today 87:187
60. Yamaguchi Y, Yasutake N, Nagaoka M (2003) J Molec Struct (THEOCHEM) 639:137
61. Bucko T, Hafner J, Benco L (2004) J Phys Chem A 108:11388
62. Demuth T, Hafner J, Benco L, Toulhoat H (2000) J Phys Chem B 104:4593
63. Bucko T, Benco L, Demuth T, Hafner J (2002) J Chem Phys 117:7295
64. Nguyen MT, Raspoet G, Vanquickenborne LG (1997) Chem Soc Perkin Trans 4:821
65. Shinohara Y, Shouro SMD, Nakajima T (2000) J Molec Struct 497:1
66. Gil A, Clotet A, Ricart JM, Kresse G, Garcia-Hernandez M, Rösch N, Sautet P (2003) Surf Sci 530:71
67. Kresse G, Gil A, Sautet P (2003) Phys Rev B 68:073401
68. Gajdos M, Hafner J (2005) Surf Sci 590:117
69. Stroppa A, Termentzidis K, Paier J, Kresse G, Hafner J (2007) Phys Rev B 76:195440
70. Uzunova EL, Kresse G, Hafner J (2007) J Chem Phys (submitted)
71. Ianuzzi M, Laio A, Parrinello M (2003) Phys Rev Lett 90:238302